Hierarchically distributed microstructure design of haptic sensors for personalized fingertip mechanosensational manipulation

Liao, Xinqin; Wang, Wensong; Lin, Maohua; Li, Minghua; Wu, Hualin; Zheng, Yuanjin

2018

Liao, X., Wang, W., Lin, M., Li, M., Wu, H., & Zheng, Y. (2018). Hierarchically distributed microstructure design of haptic sensors for personalized fingertip mechanosensational manipulation. Materials Horizons, 5(5), 920-931. doi:10.1039/C8MH00680F

https://hdl.handle.net/10356/137068

https://doi.org/10.1039/C8MH00680F

Journal Name

COMMUNICATION

Hierarchically distributed microstructure design of haptic sensors for personalized fingertip mechanosensational manipulation

Xinqin Liao,*[a] Wensong Wang,[a] Maohua Lin,[b] Minghua Li,[c] Hualin Wu[c] and Yuanjin Zheng*[a]

Received 00th January 20xx,
Accepted 00th January 20xx

DOI: 10.1039/x0xx00000x

www.rsc.org/

Abstract: Strategies to help reconstruct and restore haptic perception are essential for control of prosthetic limbs, clinical rehabilitation evaluation, and robotic manipulation. Here, we propose hierarchically distributed microstructure based on electric contact theory to develop haptic sensors. The sensing range of the haptic sensor based on hierarchically distributed microstructure is greatly enhanced by ten times relative to the one of the haptic sensor based on common structure. Furthermore, variation in the response signal of the haptic sensor is up to five orders of magnitude to scale with the external pressure between 0.5 and 100 kPa, which is close to the range that finger normally feels. Personalized manipulation of electrical appliances, three-dimensional passwords matrix, and gesture control of data glove demonstrate the fascinating potential of the haptic sensors for human-machine interactive system, force-enhanced security system, and wearable electrical system.

Introduction

Human skin possesses a network of mechanoreceptors that enable to translate external mechanical stimuli (pressure up to 100 kPa) into physiological signals, which are then interpreted by the brain.[1-4] The haptic perception that occurs when skin contacts with objects and then mechanoreceptors provide physical information of the objects is critical for experiencing the world around us.[5,6] The deficit of haptic perception due to human aging or disability abolishes the ability to dexterously control and manipulate objects because the brain obtains insufficient physiological signals about mechanical stimuli between the objects and fingers.[7-9] Strategies to help reconstruct and restore haptic perception are essential for control of prosthetic limbs, clinical rehabilitation evaluation, and robotic manipulation.[10-14] Rapidly developing artificial haptic sensors are motivated by these ultimate scientific and engineering goals. Mimicking the haptic perception of skin is therefore desired in electronic system especially for the intuitive feedback of human-machine interaction.[15-26] However, to date, obtaining single haptic sensor that distinguishes a wide range of pressure, such as low pressure (<10 kPa) and medium pressure (10-100 kPa), and thus can tactfully and differentially interact with objects without an extra signal optimization circuit is still challenging.

Significant progress along with the design of sensing structure has recently been achieved in the field of artificial haptic sensors to mimic the haptic perception of human skin.[27-50] Through coating composite material of silver nanowires (Ag NWs) and waterborne polyurethane over pre-strained fibers, a flexible piezoresistive sensor based on wrinkle microstructure was proposed to sensitively detect pressure and bending deformations, showing its potential for smart fabrics and wearable electronics.[37] Consisting of polyvinylidene fluoride (PVDF), polyaniline (PANI) solution and a polycarbonate track etched membrane, a self-powered sensor inspired by human mechanoreceptors was fabricated to mimic the slow- and fast-adaption of human skin, which effectively identified surface roughness as well as contact by a moving object.[38] By creating nanoscale crack junctions, modulating the crack geometry, and coating with a self-healable polymer, highly sensitive and durable crack-based sensors were fabricated to selectively recognize voice tone and detect hand movement.[51-53] Optional elastomer materials with hollow structures were widely investigated by filling varied functional materials to create non-invasive pressure-sensitive sensors.[39-45] Accordingly, the type of non-invasive sensors could detect human-related gentle pressure less than 10 kPa easily, and their applications were demonstrated as ranging from ubiquitous monitoring of wrist pulse, acoustic vibration recognition to breath detection.

[a] School of Electrical and Electronic Engineering, Nanyang Technological University, 50 Nanyang Avenue, Singapore 639798, Singapore. liaoxinqin677@163.com, yjzheng@ntu.edu.sg
[b] Department of Ocean & Mechanical Engineering, Florida Atlantic University, 777 Glades Road, Boca Raton, 33431, USA.
[c] School of Materials Science and Engineering, University of Science and Technology Beijing, 30 Xueyuan Road, Haidian District, Beijing 100083, China.
†Electronic Supplementary Information (ESI) available. See DOI: 10.1039/x0xx00000x

Additionally, inspired by epidermis microstructure, various skin-like sensors were fabricated by microstructure engineering for conceivable medical measurements and simple mapping pressure distribution.[46-50,54-58] There the sensing signals could be facilely got without any auxiliary circuits. Despite significant progress, most of sensors still required an extra signal optimization circuit of noise reduction and amplifiers for further signal triggering and action executing.[7,48,59]

Human finger skin is a multilayered organ that can distinguish external pressure stimuli by transmitting signals from the epidermis to different mechanoreceptors, including Merkel cells, Meissner corpuscle, Ruffini corpuscle and Pacinian corpuscle.[2,5,60] Inspired by this distributed sensing mechanism, herein we propose hierarchically distributed microstructure to develop haptic sensors that translate fingertip pressure input into electronic signals that extensively scale with the pressure. The pencil-drawn method, which is a practical and scalable manufacturing technique,[61-63] is used to prepare three types of haptic sensors based on different microstructures. Abrasive paper is adopted to provide a rough surface to distributedly delay the contact of conductive materials. In comparison, the range of pressure detection of the haptic sensor based on hierarchically distributed microstructure (HDM haptic sensor) is desirable and greatly enhanced by ten times relative to the one of the haptic sensor based on flat structure (FS haptic sensor) and extended by 100% compared to the one of the haptic sensor based on surface microstructure (SM haptic sensor). The broader range of pressure detection is attributed to adopting the design of the hierarchically distributed microstructure based on the electric contact theory.[64] Remarkably, the variations in the normalized current of the HDM haptic sensor is up to five orders of magnitude to respond to the external pressure between 0.5 and 100 kPa, which is close to the range that human finger could normally feel.[34] Importantly, the HDM haptic sensor realizes stable and long-term monitoring of gentle touch (<10 kPa) and medium-pressure regime (10-100 kPa).[4,65] To better describe the specific magnitude of medium pressure, the ranges of 10-50 kPa and >50 kPa were further expressed as long click and heavy press, respectively, in this work. Through the analysis and processing of data without any denoising, signal amplifying, and baseline tracking, only one HDM haptic sensor possesses the ability to discriminatively control the switch of three different types of electrical appliances, including desk lamp, electric fan, and computer screen. Furthermore, three-dimensional (3D) password matrix is demonstrated by integrating with the HDM haptic sensors to promote force-enhanced security system to a new level. Besides, through Bluetooth communication technology, the HDM haptic sensors endow a glove with a wireless gesture-controlling function, showing their potential in the field of fascinating wearable interactive entertainment system. We believe that the hierarchically distributed microstructure puts forward a novel design thought and a scalable approach to develop haptic sensors, and may further advance the haptic sensors based on other sensing principles, such as capacitance sensing, piezoelectric sensing, and triboelectric sensing.

Results and discussion

Conductive graphite can be easily deposited on a rough substrate by the pencil-drawn method, which is a practical and scalable manufacturing technique.[61-63] In order to prepare the conductive substrate with apparent undulation microstructure like epidermis microstructure,[2,5,60] commercial abrasive paper composed of numerous abrasives and brown paper was used as the substrate (**Fig. S1**, **ESI†**). The fabrication process of the haptic sensor based on hierarchically distributed microstructure (HDM haptic sensor) is illustrated in **Fig. 1a**. Firstly, the abrasive paper was patterned by adhesive tape to reserve the area for depositing graphite. The pencil has been used to effectively fabricate various electronics,[63] which were based on the good electric conductivity of pencil trace that was a nanocomposite of graphite and intercalated clay. Through the simple and effective pencil-drawn method, graphite slices were layered or peeled from a 9B pencil and then deposited on the patterned abrasive paper to form a conductive graphite film. At the second stage, another adhesive tape was introduced to stick on the graphite film with a gentle pressure by using a squeegee. It should be noted that the pressure applied here was to make the graphite slices interconnect together on the adhesive tape after peeling off it. As graphite was layered and easily mechanically exfoliated,[66] the abrasive paper still stored enough graphite slices to be conductive. Subsequently, the adhesive tape with graphite film and the abrasive paper with remaining graphite film face-to-face sandwiched an electric wire, which served as a spacer. Finally, two of these combinations were assembled and encapsulated together to form the HDM haptic sensor. More details can be found in the section of Methods.

The morphology of the surfaces of these three different conductive substrate materials, including the abrasive paper with fresh graphite film, the abrasive paper with remaining graphite film, and the adhesive tape with graphite film, were observed by field emission scanning electron microscopy (FESEM). **Figure 1b** shows that obvious bump cannot be observed on the surface of the abrasive paper with fresh graphite film, which is prepared by pencil drawing without any postprocessing. Further verification was conducted by the surface profiler. Although the surface roughness of the pure abrasive paper was up to 18.5 μm, the surface of the abrasive paper with fresh graphite film was almost flat in the micro level (**Fig. S2a and S2b**, **ESI†**), which was contributed to the smoothness and adhesion of pencil trace. After pasting and peeling off adhesive tape, a micropatterned surface was generated on the abrasive paper as shown in **Fig. 1c**, where abundant bumps were clearly observed, indicating that the abrasives still be coated with graphite slices. Correspondingly, graphite slices were interconnected with each other to generate microgroove on the surface of the substrate that is the adhesive tape with graphite film (**Fig. 1d**). Notably, the surface roughness of the abrasive paper with remaining graphite film and the one of the adhesive tape with graphite film were similar (**Fig. S2c** and **S2d**, **Fig. S3a** and **S3b**, **ESI†**). Both of their surfaces were rougher than that of the abrasive paper with fresh graphite film (**Fig. S2b** and **Fig. S3c**, **ESI†**). The conductive

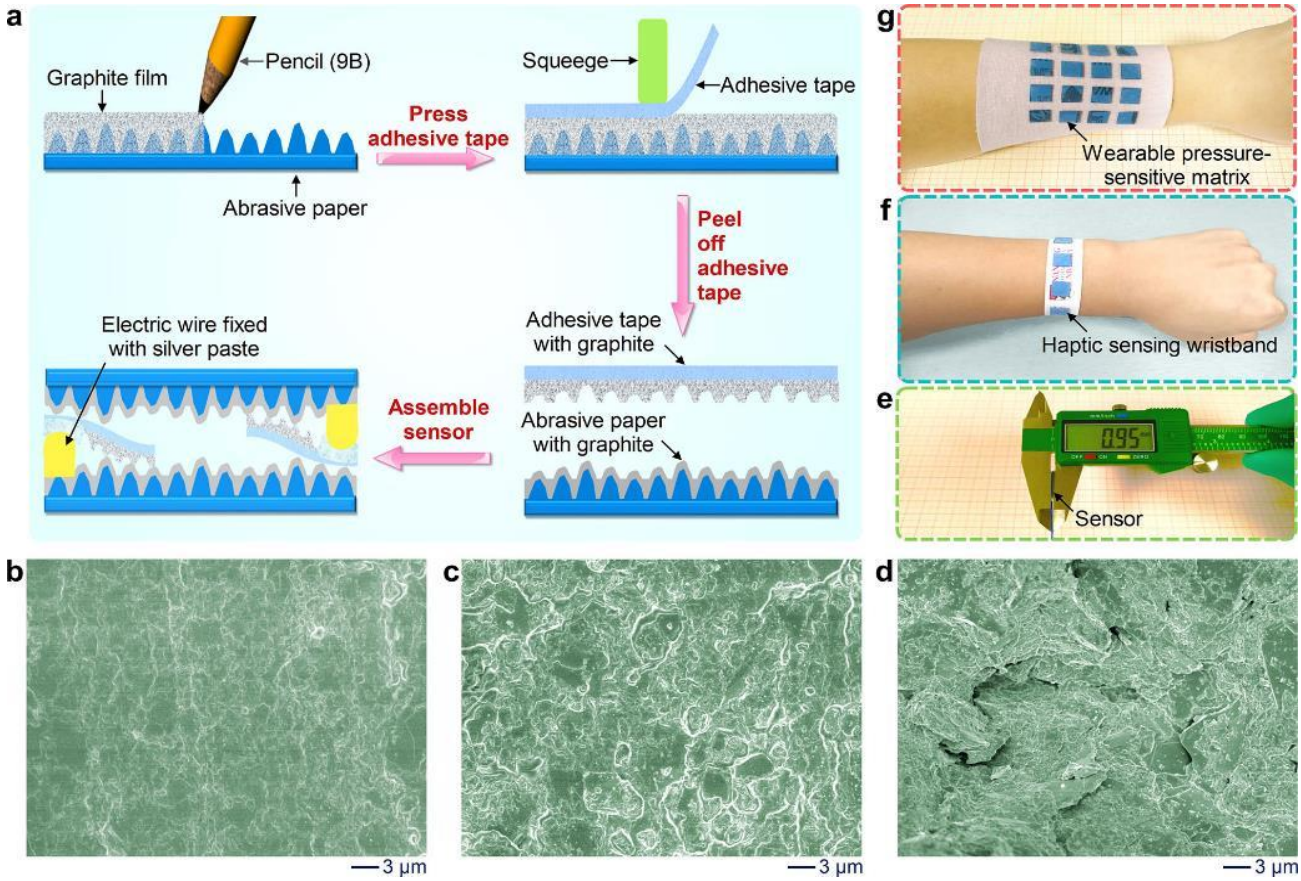

Fig. 1 | Construction and characterization of haptic sensors. (**a**) Schematic illustration of the haptic sensor based on hierarchically distributed microstructure (HDM haptic sensor). (**b**) Field emission scanning electron microscopy (FESEM) image of the surface of the abrasive paper with fresh graphite film. (**c**) FESEM image of the surface of the abrasive paper with remaining graphite film after peeling off adhesive tape. (**d**) FESEM image of the surface of the adhesive tape with graphite film. (**e**) The thickness measurement of HDM haptic sensor, which showed the thickness was 0.95 mm. (**f**) Photograph of a multipoint haptic sensing wristband integrated with HDM haptic sensors. (**g**) Photograph of a wearable pressure-sensitive matrix integrated with HDM haptic sensors over an arm.

substrate materials with different surface roughness provided the comparability of microstructure engineering for the later construction of different types of haptic sensors. In the following experiments, we found that the rough surface contributed to the distributed contact delay of conductive materials, and thus the sensing range of haptic sensors would be extended. As shown in **Fig. 1e**, the as-prepared HDM haptic sensor was thin and could be integrated as a multipoint haptic sensing wristband (**Fig. 1f**) and a wearable pressure-sensitive matrix on the arm (**Fig. 1g**), implying its potential applications for human-machine interactive systems in the future.

For comparison, three types of haptic sensors were prepared (**Fig. 2a**). The haptic sensor based on flat structure (FS haptic sensor) was made of the abrasive papers with fresh graphite film. In the second case, two abrasive papers with remaining graphite film were face-to-face put together for fabricating the haptic sensor based on surface microstructure (SM haptic sensor). It should be pointed out that these two types of haptic sensors featured upper and bottom layered structures, which both sandwich two spacers. As a contrast, the as-prepared haptic sensors were all in size of 10 × 10 mm^2. **Figure S4** in **ESI†** shows that the three types of haptic sensors all belong to resistance-type devices. To investigate the properties, the variations of resistance of the FS haptic sensor, SM haptic sensor, and HDM haptic sensor were measured by different external force, as shown in **Fig. 2b**. Based on the design of devices, all the haptic sensors were non-conductive when no external force was applied, owing to the fact that the upper and bottom layers of devices were slightly separated by the spacers. They would become conductive when gentle force was applied. Their resistance would significantly decrease with the increased external force. The results showed that all the as-prepared haptic sensors provided technical self-switching function, which was important for energy conservation when no external force was applied. The onset resistance, which was the thresholds that was defined as the resistance of the haptic sensors begun to decrease obviously, occurred at the external force of 0.01, 0.02, and 0.05 N corresponding to the FS haptic sensor, SM haptic sensor, and HDM haptic sensor, respectively. The larger onset detection of force was attributed to the higher separation distances of the upper and bottom layers of the HDM haptic sensor, which contained an extra internal conductive substrate. It was noteworthy that the FS haptic sensor showed the lower resistance relative to the one of the other two types of haptic

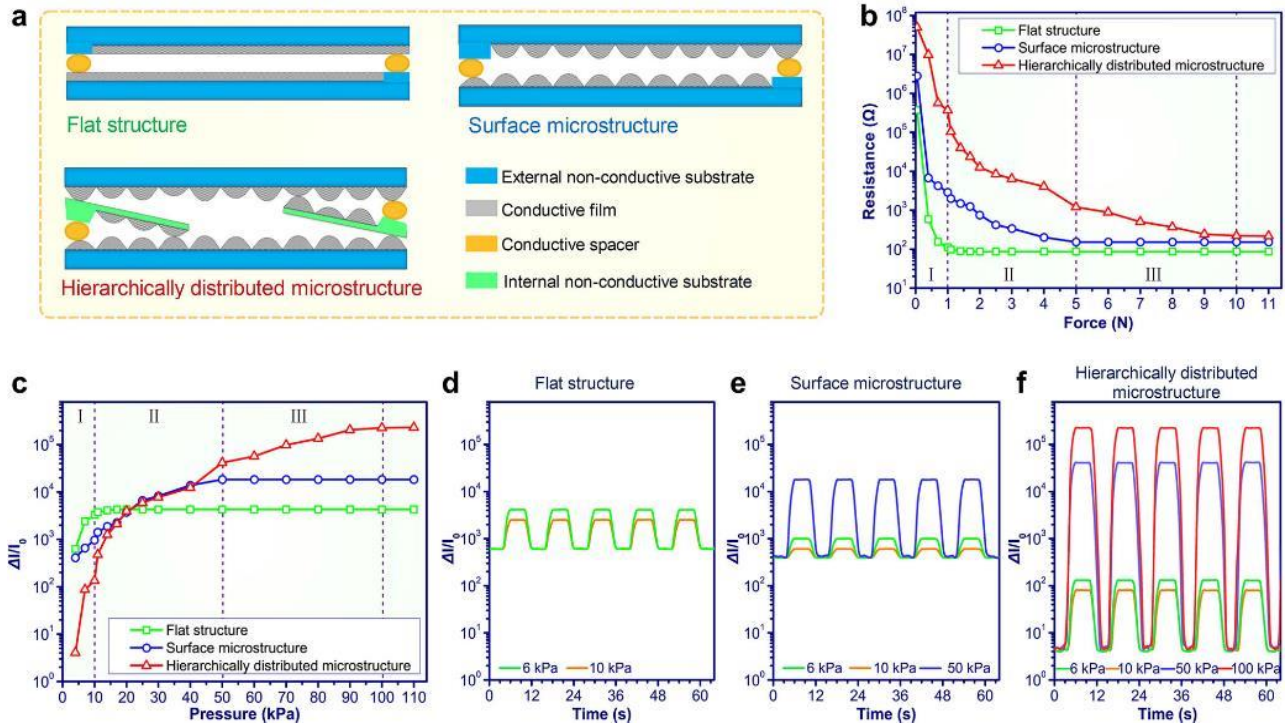

Fig. 2 | Properties of haptic sensors. (**a**) Three types of the structure diagram of haptic sensors based on flat structure (FS), surface microstructure (SM), and hierarchically distributed microstructure (HDM), respectively. (**b**) Typical resistance of the FS haptic, SM haptic sensor, and HDM haptic sensor *versus* force. (**c**) Variation in the normalized current of the three types of haptic sensors under different pressure. (**d-f**) Current responses of the three types of haptic sensors corresponding to dynamic pressure with the loading-unloading process.

sensors at the same applied external force. In simple terms, the resistance of the haptic sensors depended on the degree of difficulty of electron movements, which was affected by the surface roughness of the conductive substrates. The above results showed that the surfaces of the abrasive paper with remaining graphite film and the adhesive tape with graphite film were rougher than that of the abrasive paper with fresh graphite film (**Figs. S2b-d** and **Fig. S3**, **ESI†**), which thus would make the electron movements more difficult and prolong the conductive path between the electrodes. Accordingly, the resistance of the FS haptic sensor was relatively lower than that of other two types of haptic sensors at the same external force. Specifically, the resistance of the FS haptic sensor was not varied after the external force exceeded 1 N, indicating that the device characterized a corresponding force detection limit of 1 N. For the SM haptic sensor, the force detection limit reached up to 5 N that was 5 times larger than the one of the FS haptic sensor. The larger detection range of the SM haptic sensor was mainly due to the contact areas of the upper and bottom layers that were the abrasive papers with remaining graphite film increased slowly with the external force. As the change of contact area would affect the conductive paths between the upper and bottom layers, the resistance of the SM haptic sensor was not fixed until the contact area tends to saturation. This was unlike the contact of the upper and bottom layers of the FS haptic sensor, which adopted the abrasive papers with fresh graphite film as conductive substrate. For the FS haptic sensor, the contact of each area was finished in one step to respond to the external force, and would not be further dramatically changed with the increase of the external force. Other study also found the similar extension of detection range through introducing the microstructure of pyramid.[47] Through hierarchically distributed microstructure design, the resistance of the HDM haptic sensor would not tend to be constant until the external force exceeded 10 N. The results indicated that by means of roughening the conductive surface, the detection range of the device would be increased. A further increase of the detection range could be achieved through hierarchically distributed microstructure design. In detail, the force detection range of the HDM haptic sensor was increased by 100% compared to the one of the SM haptic sensor, and was 10 times wider than that of the FS haptic sensor. The larger detection range will provide the foundation for more fruitful applications of haptic sensors in the future, especially for personalized fingertip mechanosensational manipulation. Meanwhile, the design thought of this hierarchically distributed microstructure may further promote the development of haptic sensors based on other sensing principles, such as capacitance sensing, piezoelectric sensing, and triboelectric sensing.

Figure 2c shows the variations in the normalized current ($\Delta I/I_0$, where ΔI is the relative change in current and I_0 is the current of the haptic sensors under the pressure of 0.5 kPa) of the three types of haptic sensors under different pressure. The current signal of the FS haptic sensor could not distinguish the pressure of >10 kPa. This was because the resistance of the FS haptic sensor did not change further when the force was larger

than 1 N, as shown in **Fig. 2b**. Thus, when the applied voltage of 5 V became stable, the variation in the normalized current would not rise even if pressure increased. Similarly, the current signal of the SM haptic sensor was stationary after the pressure increases beyond 50 kPa. In comparison, the pressure detection limit of the HDM haptic sensor was as high as 100 kPa, which was close to the range that human finger could normally feel.[34] Importantly, the change of the normalized current of the HDM haptic sensor was up to five orders of magnitude to respond to the external pressure, which could facilitate a significant reduction of the difficulty in the back-end signal processing, and provide an advantage to simplify the circuit. This is particularly important for the integration system with numerous devices in the future. Therefore, the resulting HDM haptic sensor was advanced for human-machine interactive system, which would be demonstrated in the following section of applications. **Figures 2d-f** show the current responses of the three types of haptic sensors under dynamic pressure. Variation in the normalized current of the FS haptic sensor was tested in the pressure of 6 and 10 kPa (**Fig. 2d**). The result showed the electrical response of the FS haptic sensor was consistent throughout the loading-unloading process. **Figure 2e** indicates that the continuous variations in the normalized current of the SM haptic sensor can be obtained, which are synchronized with the applied pressure of 6 and 10 kPa and even up to 50 kPa. Furthermore, it could be clearly observed that the dynamic changes in the wider range of pressure between 6 and 100 kPa were identified by the HDM haptic sensor, which was contributed to the hierarchically distributed microstructure design (**Fig. 2f**). The results clearly manifested that using pencil drawn on the abrasive paper could construct ideal haptic sensors with switch function and stable electromechanical response performance. The fabrication strategies are practical, effective, and scalable. Specially, through microstructure engineering design, the detection range of haptic sensors will be significantly expanded due to the increase of surface roughness of conductive substrate. Importantly, adopting hierarchically distributed microstructure design can make the further enlargement of the detection range of haptic sensors, almost reaching the pressure sensing range of human fingers.

To understand the working mechanism, **Figure 3** illustrates the sensing schematic diagrams and simplified equivalent circuit diagrams of the three types of haptic sensors. Based on our design, the initial upper and bottom layers of the FS haptic

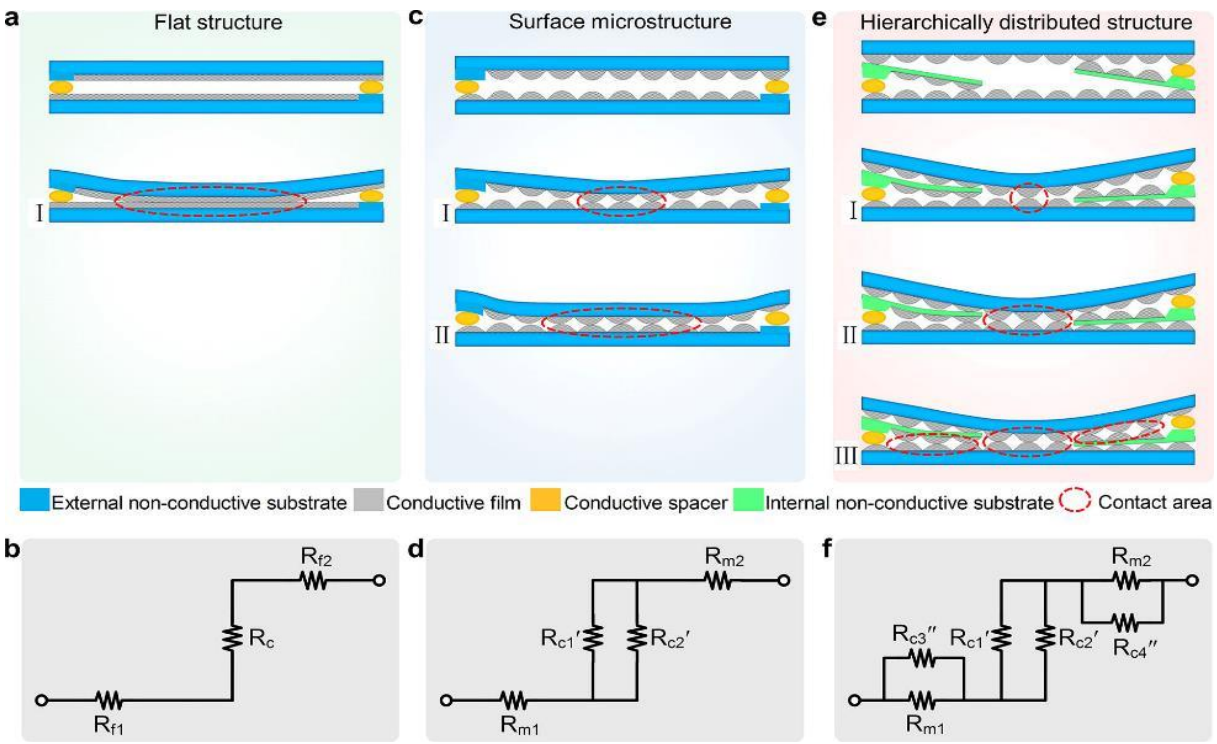

Fig. 3 | Transduction mechanism of haptic sensors. (**a**) Schematic diagram of sensing mechanism of the FS haptic sensor. (**b**) Simplified equivalent circuit diagram of the FS haptic sensor. R_{f1} and R_{f2} are the resistance of the upper and bottom conductive flat substrate, respectively. R_c is the contact resistance of the interfaces between the upper and bottom conductive flat substrate. (**c**) Schematic diagram of sensing mechanism of the SM haptic sensor. (**d**) Simplified equivalent circuit diagram of the SM haptic sensor. R_{m1} and R_{m2} are the resistance of the upper and bottom conductive microstructure substrate, respectively. R_{c1}' and R_{c2}' are the contact resistance of the interfaces between the upper and bottom conductive microstructure substrate under gentle and medium force, respectively. (**e**) Schematic diagram of sensing mechanism of the HDM haptic sensor. (**f**) Simplified equivalent circuit diagram of the HDM haptic sensor. R_{c3}'' is the contact resistance of the interfaces between the bottom and internal conductive microstructure substrate. R_{c4}'' is the contact resistance of the interfaces between the upper and internal conductive microstructure substrate.

sensor are non-contacted under the unloading external force (**Fig. 3a**). As a gentle force is applied, the contact between the top and bottom layers using conductive flat substrates exhibits sharp increase in each area, and will not be further dramatically changed with the increase of external force, owing to the fact that there is no additional substructure to be further contacted (**Fig. 3aI**). Therefore, the total resistance (R_t) can be simplified as: $R_t = R_{f1} + R_{f2} + R_c$, where R_{f1} and R_{f2} are the resistance of the upper and bottom conductive flat substrates, respectively, R_c is the contact resistance of the interfaces between the upper and bottom conductive flat substrates (**Fig. 3b**). For the SM haptic sensor, the contact between the top and bottom layers using conductive microstructure substrates is generated under a gentle force (**Fig. 3cI**). Due to the presence of the substructure of rough surface, the contact of conductive materials will be distributedly delayed. The number of contact points will be increased with the enlarged force, resulting in the augmentation of contact areas and thus increasing more conductive paths (**Fig. 3cII**). The electric contact theory indicates that when two conductors are in contact with each other, the contact resistance will change with the variation of the contact area.[64] Accordingly, the total resistance of the SM haptic sensor will further decrease, which is attributed to the fact that more conductive paths are in parallel. At this case, the total resistance will not vary until all the contact points reach saturation, showing the larger detection range than the one of counterpart using flat structure. As shown in **Fig. 3d**, the total resistance of the SM haptic sensor can be simplified as: $R_t = R_{m1} + R_{m2} + R_{c1}'R_{c2}'/(R_{c1}' + R_{c2}')$, where R_{m1} and R_{m2} are the resistance of the upper and bottom conductive microstructure substrates, respectively, R_{c1}' and R_{c2}' are the contact resistance of the interfaces between the upper and bottom conductive microstructure substrates under gentle and medium force, respectively.

We know human skin is multilayer organ that can distinguish external pressure stimuli by transmitting signals from the epidermis to different mechanoreceptors, including Merkel cells, Meissner corpuscle, Ruffini corpuscle and Pacinian corpuscle.[2,5,60] Inspired by this distributed sensing mechanism, herein we propose hierarchically distributed microstructure to make a breakthrough of the detection range of haptic sensors. **Figure 3e** shows the schematic diagram of sensing mechanism of the HDM haptic sensor. Basically, this device senses external forces through two different sensing units. The sensing unit based on the contact state between the external conductive layers with surface microstructure is used to detect the gentle and medium force. When a gentle force is applied to the HDM haptic sensor, the two external layers first will contact (**Fig. 3eI**). As the statement of the electric contact theory above, the resistance of the device decreases with the increase of the

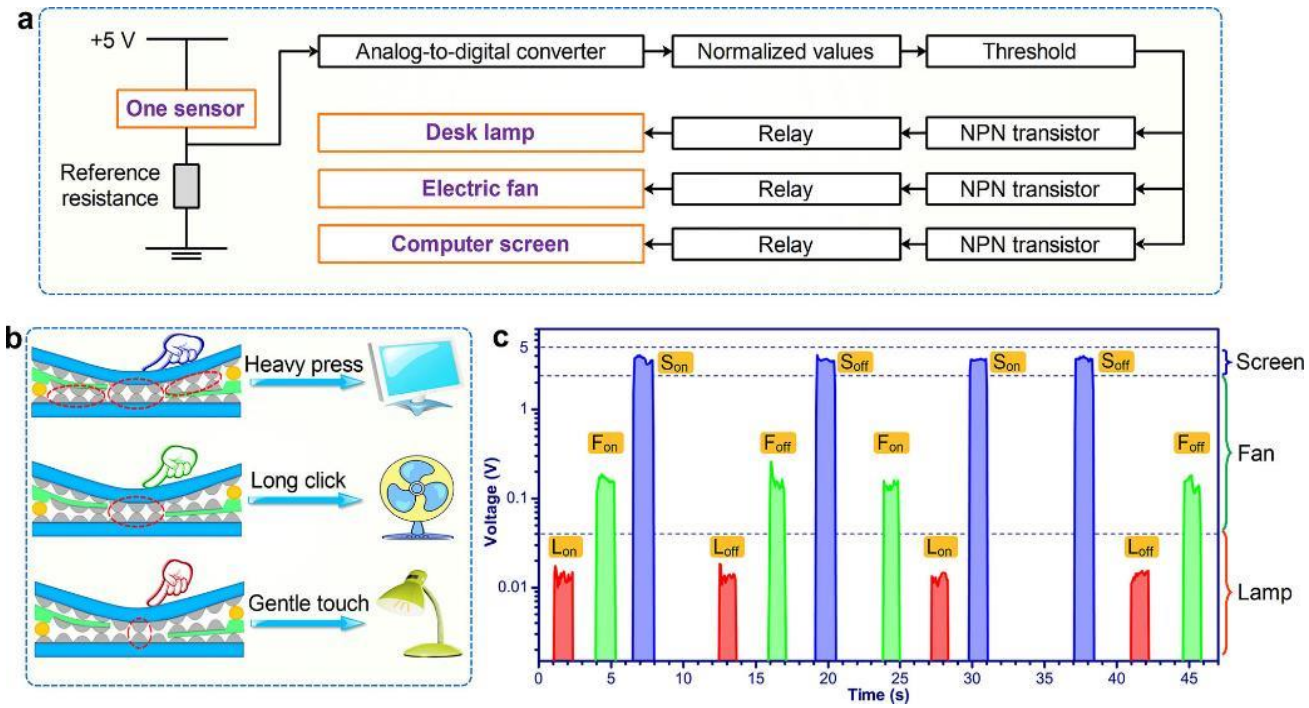

Fig. 4 | Application for discriminative control of different electrical appliances based on only one haptic sensor. (**a**) Circuit flowchart of the HDM haptic sensor used to discriminatively control desk lamp, electric fan, and computer screen. (**b**) Schematic diagram of one HDM haptic sensor used to discriminatively control the switch of the desk lamp, electric fan, and computer screen by gentle touch, long click, and heavy press, respectively. (**c**) Voltage response related to the HDM haptic sensor, which is subjected to different fingertip force. L_{on} and L_{off} represent sending instructions to turn the lamp on and off, respectively. F_{on} and F_{off} are the instructions that turn the fan on and off, respectively. S_{on} and S_{off} are the instructions to open and close the screen, respectively.

number of contact points, resulting from the larger force (**Fig. 3eII**). The further increasing force is detected by the other sensing unit, which is based on the contact state between the external and internal conductive layers with surface microstructure (**Fig. 3eIII**). Until all possible contact points are saturated, the resistance of HDM haptic sensor does not decrease. The simplified equivalent circuit diagrams of the HDM haptic sensor corresponding to three different states are illustrated in **Fig. S5**, **ESI†**. Thus, the total resistance of the HDM haptic sensor can be expressed as: $R_t = R_{m1}R_{c3}''/(R_{m1} + R_{c3}'') + R_{m2}R_{c4}''/(R_{m2} + R_{c4}'') + R_{c1}'R_{c2}'/(R_{c1}' + R_{c2}')$, where R_{c3}'' is the contact resistance of the interfaces between the bottom and internal conductive microstructure substrate, R_{c4}'' is the contact resistance of the interfaces between the upper and internal conductive microstructure substrate. As a result, although the detection range of HDM haptic sensor is limited, it is much larger than that of the simple haptic sensor based on the upper and bottom layered structure, which is matched with the experimental results in **Fig. 2**.

In general, a switch only controls an electrical appliance. As results mentioned above, the HDM haptic sensor not only featured switch function, but also characterized the wide variation range of the electrical signal, which was up to five orders of magnitude to respond to the external pressure between 0.5 and 100 kPa. In this study, we constructed a smart branch console system of multiple electrical appliances based on only one HDM haptic sensor. **Figure 4a** is the circuit flowchart of the smart branch console system with the HDM haptic sensor, which is used to discriminatively control desk lamp, electric fan, and computer screen. The operating voltage was 5V and the resistor of 1800 Ω was selected as the reference resistance. We set the pressure below 10 kPa as gentle touch, specified that the pressure of long click was between 10 and 50 kPa, and defined it as the heavy press when the pressure exceeded 50 kPa. Since each allocated pressure range of these motions was wide enough, the expected event could be easily imported by fingertip. As shown in **Fig. 4b** and **Fig. S6**, **ESI†**, the "on" and "off" states of desk lamp, electric fan, and computer screen were independently manipulated by the gentle touch,

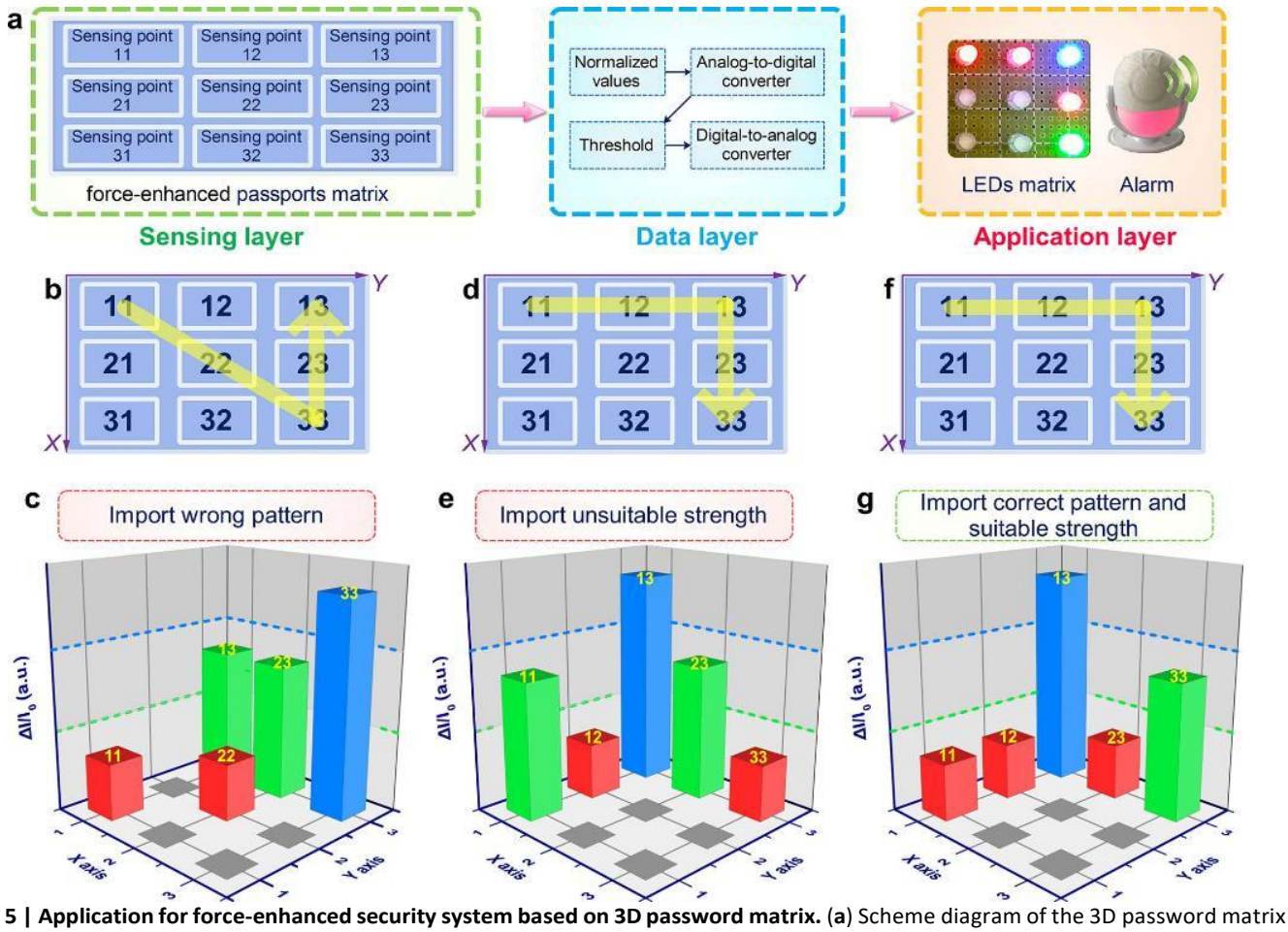

Fig. 5 | Application for force-enhanced security system based on 3D password matrix. (**a**) Scheme diagram of the 3D password matrix integrated with nine HDM haptic sensors. Illustrations of the fingertip pressing on the HDM haptic sensors along the paths: (**b**) 11 → 22 → 33 → 23 → 13, (**d**, **f**) 11 → 12 → 13 → 23 → 33. (**c**, **e**, **g**) Electrical responses recorded from the force-enhanced 3D password matrix when the fingertip pressed on each HDM haptic sensor.

long click, and heavy press, respectively. When a user finger gently touched on the HDM haptic sensor, electrical signal was generated quickly (**Fig. 4c**). After the electrical signal lasted for the set time of 800 ms, a switch instruction would control the operation of the desk lamp. Furthermore, once the HDM haptic sensor perceived the pressure of long click from the user's fingertip over 800 ms, assigned transistor would send the instruction of "turn on" or "turn off" to the electric fan. Besides, the HDM haptic sensor exhibited the relatively high electrical signal to mechanical fingertip event of heavy press. Through the heavy press, the state of the computer screen would be changed. A series of tests manifested the reliable performance of the HDM haptic sensor and demonstrated that fingers could control different electrical appliances easily and individually by using only one HDM haptic sensor (**Movie S1**, **ESI†**). Notably, owing to the wide variation range of the electrical signal, large sensing range of pressure, reproducible pressure response (**Fig. S7**, **ESI†**), and stable performance of long-term pressure detection (**Fig. S8**, **ESI†**), the signal processing of the HDM haptic sensor did not include any denoising, signal amplifying, and baseline tracking. It could facilitate a significant reduction of the difficulty in the signal processing, and specially would offer a unique advantage to simplify the circuit design of the integration system with numerous devices in the future.

Security passwords have penetrated into every corner of our lives. The rapid development of password cracking technique makes people feel uneasy about their property and privacy. In the following study, we developed force-enhanced security system based on the three-dimensional (3D) password matrix integrated with nine HDM haptic sensors (**Fig. 5** and **Fig. S9a**,

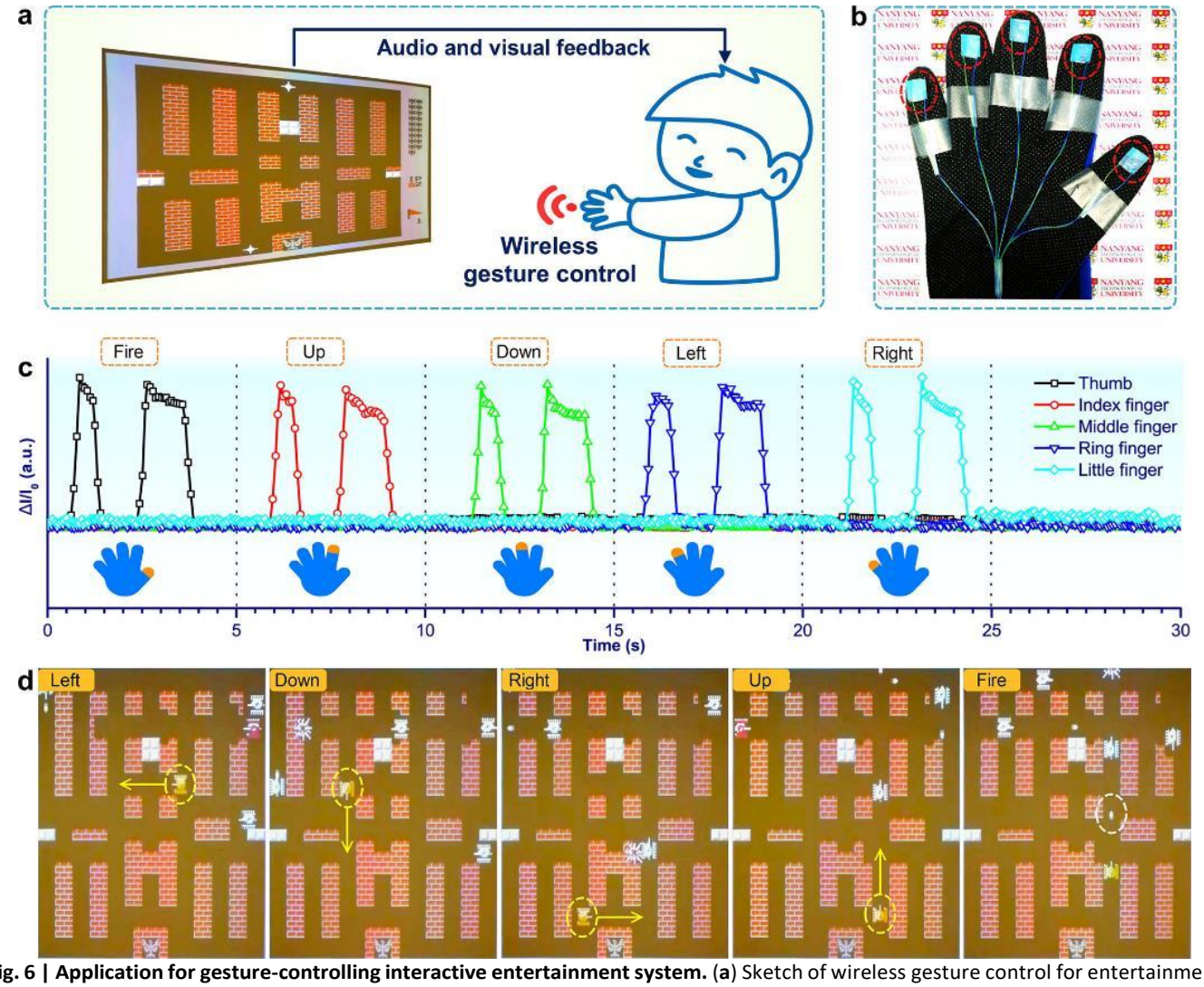

Fig. 6 | Application for gesture-controlling interactive entertainment system. (**a**) Sketch of wireless gesture control for entertainment interaction. (**b**) Photograph of the data glove integrated with five HDM haptic sensors onto each glove finger, Insets of red dotted circles point out each HDM haptic sensor. (**c**) Correspondence between electrical signals and instructions in the intelligent gesture-controlling interactive entertainment system. (**d**) Demo of a game tank with "left", "down", "right", "up", and "fire" instructions, where the actions of the game tank are pointed out by a yellow dotted circle with an arrow and a white dotted circle.

ESI†). The typical variations of resistance of multiple HDM haptic sensors under different external force were shown in **Fig. S10**, **ESI†**, which indicated the similar variation trend of the sensing performance of these HDM haptic sensors. Traditionally, each point of common password matrix only has two states of "0" and "1". As the results mentioned above, the HDM haptic sensor could easily identify four kinds of pressure, including no pressure, gentle touch, long click, and heavy press. Thus, we could define four states of each HDM haptic sensor as "0", "1", "2", and "3" corresponding to the no pressure, gentle touch, long click, and heavy press, respectively. Just to make a simple comparison, a password is composed of five points, such as point 1, point 2, point 3, point 4, and point 5. Pressing these five points in the correct sequence by anyone's fingers will turn out the password from common password matrix. However, the 3D password matrix integrated with the HDM haptic sensors will give 3^5 combinations of the same order. So, it can be inferred that the security system would be pushed to a new level by using the 3D password matrix integrated with the HDM haptic sensors. As a proof-of-concept demonstration, **Figure 5a** schematically describes a 3D password matrix consisting of 3 × 3 HDM haptic sensors. Through the analysis and processing of data layer, the acquisition of fingertip pressure from the sensing layer would be expressed into the visible color of light-emitting diode (LED: full color, four legs with a common cathode). In detail, the gentle touch, long click, and heavy press would make the LED emit red, green, and blue light, respectively. In this work, the password of the 3D password matrix was set as 11 (gentle touch) → 12 (gentle touch) → 13 (heavy press) → 23 (gentle touch) → 33 (long click). Incorrect import, including pressing the correct pattern with unsuitable force strength, would make the alarm work in the application layer. For example, when a tester's fingertip pressed on the HDM haptic sensors along the path: 11 (gentle touch) → 22 (gentle touch) → 33 (heavy press) → 23 (long click) → 13 (long click) (**Fig. 5b**), the electrical signals from the force-enhanced 3D password matrix were recorded in **Fig. 5c**. Correspondingly, the LEDs matric imparted the human-readable response of the importing process (**Fig. S9b**, **ESI†**). As the wrong pattern was imported, the alarm sent out acousto-optic warning (**Movie S2**, **ESI†**). When the correct pattern was imported by the tester's fingertip along the path: 11 (long click) → 12 (gentle touch) → 13 (heavy press) → 23 (long click) → 33 (gentle touch) (**Fig. 5d**), the electrical response from the force-enhanced 3D password matrix showed the pressure from fingertips on each sensing point (**Fig. 5e**), which was also explicitly reflected by the LEDs matrix (**Fig. S9c**, **ESI†**). As set above, the suitable strength of the sensing point 11 should be imported by the gentle touch. However, in this time, fingertip pressure applied to the sensing point 11 was imported by the long click, which was unsuitable strength. In the same situation, the pressure strength applied to the sensing point 23 and sensing point 33 was also unsuitable in this import. Therefore, the alarm also worked on this occasion due to the unsuitable strength import. Only importing correct pattern and suitable strength did not make the alarm work in the application layer (**Figs**. **5f**, **5g** and **Fig. S9d**, **ESI†**). The results showed that the force-enhanced security system integrated with the HDM haptic sensors could bring a safer to our lives, where the leakage of the numbers of passwords would not make people uneasy.

It is of significant interest that gestures will play promising and meaningful roles and analog-nature communication interfaces between machine and people. As a proof of concept, in **Fig. 6**, we demonstrated the practical capability of the HDM haptic sensors towards intelligent gesture-controlling interactive entertainment system. Audio and visual feedback would provide indirect information about the gesture (**Fig. 6a**). We carried out this demonstration of the gesture control by using a data glove integrated with five HDM haptic sensors on each fingertip to play a Battle City game (classic 90 version), as shown in **Fig. 6b**. The flow chart of the wearable wireless interactive entertainment system consisting of five HDM haptic sensors was shown in **Fig. S11**, **ESI†**. As the drop time and rise time of the HDM haptic sensor were 21 ms and 22 ms, respectively (**Fig. S12**, **ESI†**), the fast response time would not affect common operations of the gesture control. Additionally, the HDM haptic sensor could still sense the changes of external force when it was slightly bended (**Fig. S13**, **ESI†**). Integration of five HDM haptic sensors created a data glove for detecting gesture, which was realized by pressing the HDM haptic sensor on an object (such as a table) of each fingertip. As a further detail, once the thumb of the data glove contacted the table, the microprogrammed control unit (MCU) would detect the electrical signal change from the HDM haptic sensor, which was attached on the thumb tip of the data glove. Through the signal processing including analog-to-digital conversion, normalized values, compared with threshold, digital-to-analog conversion, and Bluetooth communication technology, the functional instruction of "fire" was then transmitted to the software of Battle City game to control the action of the game tank. In this way, the data glove could detect and distinguish the pressure of each finger individually and precisely through the multichannel measurement of the HDM haptic sensors (**Fig. 6c**), and then turned the pressure from thumb, index finger, middle finger, ring finger, and litter finger into the functional instructions of "fire", "go up", "go down", "go left", "go right", respectively, to control the actions of the game tank (**Fig. 6d** and **Movie S3**, **ESI†**). We believe that through integrating with the HDM haptic sensors, versatile applications of wearable fingertip mechanosensational interaction, such as drone and prosthesis control, would spring forth to make our lives more fascinating.

Conclusions

In summary, inspired by the distributed sensing mechanism of human skin, we proposed hierarchically distributed microstructure based on electric contact theory to develop haptic sensors. Three types of haptic sensors based on different microstructures were prepared by the practical and scalable method of pencil drawing. All the as-prepared haptic sensors provided self-switching function, which was conducive to energy conservation when no external force was applied. The abrasive paper was adopted to provide a rough surface to distributedly delay the contact of conductive materials. The sensing range of the haptic sensor by microstructure

engineering design was extended five times relative to the one of the counterpart due to the effect of the distributed contact delay. Based on the hierarchically distributed microstructure, the further increased value of 100% was achieved and thus made the sensing range of the haptic sensor reach up to 100 kPa, which was close to the range that human finger could normally feel. Notably, variation in the response signal of the haptic sensor was up to five orders of magnitude to scale with the external pressure. It could facilitate a significant reduction of the difficulty in the back-end signal processing and thus provide an advantage to simplify the circuit, especially for the integration system with numerous devices in the future. The as-prepared haptic sensor also featured long-term and stable monitoring and fast response for operations. Personalized manipulation of different electrical appliances, three-dimensional password matrix, and gesture control of data glove demonstrated the fascinating potential of the haptic sensor for human-machine interactive system, force-enhanced security system, and wearable electrical system. We believe that this study puts forward a novel design thought and a scalable approach to develop haptic sensors, and may further advance the haptic sensors based on other sensing principles, such as capacitance sensing, piezoelectric sensing, and triboelectric sensing.

Experimental section

Materials and Devices Fabrication: Firstly, clean abrasive paper (MATADOR, P220) was patterned by adhesive tape (ScotchTM Magic Tape 810#, 3M Inc.) to reserve area for depositing graphite. The size of the reserved area was 10 × 10 mm^2. Then, a carbon pencil (Deli Company, 9B) drawing in horizontal direction was not employed until the graphite slices fully covered on the reserved area. After pencil drawing, a smooth conductive graphite film was deposited on the abrasive paper, marked as Substrate 1#. Second, a new adhesive tape was attached on the graphite film with a gentle pressure by using a squeegee. The semi-transparent adhesive tape would turn into being black after being applied the gentle pressure, which meant that the adhesive tape was completely attached to the graphite film. After peeling off the adhesive tape, the graphite slices were interconnected together to form another graphite film on the adhesive tape. The adhesive tape with graphite film and the abrasive paper with remaining graphite film were marked as Substrate 2# and Substrate 3#, respectively. As graphite was layered and easily mechanically exfoliated,[66] the roughness of the Substrate 2# or Substrate 3# would not be drastically changed when the slight peeling force was between 0.02-0.07 N (**Fig. S14**, **ESI†**). To fabricate the haptic sensor based on flat structure (FS haptic sensor), a copper wire was fixed on the edge of the Substrate 1# by conductive silver paint (SPI, YFS-05002). Subsequently, a spacer was formed when an adhesive tape with the size of 2 × 10 mm^2 stuck on the copper wire. Finally, two Substrates 1# with the spacer were face-to-face put together and then encapsulated by the adhesive tape. It should be noted that the two spacers were located on the opposite edge of the FS haptic sensor. For the haptic sensor based on surface microstructure (SM haptic sensor), the fabrication steps were the same as the one of FS haptic sensor except for using Substrate 3# instead of Substrate 1#. For the case of constructing the haptic sensor based on hierarchically distributed microstructure (HDM haptic sensor), the spacer was formed on the Substrate 3#. Then, the Substrate 2# with the size of 4× 10 mm^2 was put over the Substrate 3# and tilted on the spacer. These two substrates were fixed together by adhesive tape to turn into a composite structure. Finally, two such composite structures were face-to-face stuck together by adhesive tape. Notably, the two spacers were located on the opposite edge of the HDM haptic sensor.

Properties Measurements and Characterization: The morphology of substrates was observed by field emission scanning electron microscopy (JEOL, JSM 6340F) and atomic force microscope (Bruker Dimension Icon). The surface roughness profiles of substrates were characterized by Dektak XT surface profiler. The electromechanical properties and resistive responses of the haptic sensors were measured by the standard digital multimeter (UNIT UT39B), semiconductor characterization system (Keithley 4200A-SCS), and high precision digital multimeter (Agilent 34461A). The external force was obtained by a designed actuator (Beijing Times Brilliant Electric Technology Co., Ltd.) and calibrated by the standard force sensor (Bengbu Sensors System Engineering Co., Ltd., JHBM-7). The peeling force was detected by the drawing force transducer (Bengbu Sensors System Engineering Co., Ltd., JLBS-A). The thickness of device was measured by vernier caliper (HANS.w, HS1044A). Digital signals and analog signals were converted by a microprogrammed control unit (MCU, Arduino MEGA 2560).

Conflicts of interest

There are no conflicts to declare.

Acknowledgements

This work was supported by the National Research Foundation of Singapore (No. NRF-CRP11-2012-01).

Notes and references

1. R. S. Johansson and J. R. Flanagan, *Nat. Rev. Neurosci.*, 2009, **10**, 345.
2. A. Chortos, J. Liu and Z. Bao, *Nat. Mater.*, 2016, **15**, 937.
3. J. E. O'Doherty, M. A. Lebedev, P. J. Ifft, K. Z. Zhuang, S. Shokur, H. Bleuler and M. A. Nicolelis, *Nature*, 2011, **479**, 228.
4. S. C. Mannsfeld, B. C. Tee, R. M. Stoltenberg, C. V. Chen, S. Barman, B. V. Muir, A. N. Sokolov, C. Reese and Z. Bao, *Nat. Mater.*, 2010, **9**, 859.
5. P. Delmas, J. Hao and L. Rodat-Despoix, *Nat. Rev. Neurosci.*, 2011, **12**, 139.
6. S. H. Woo, S. Ranade, A. D. Weyer, A. E. Dubin, Y. Baba, Z. Qiu, M. Petrus, T. Miyamoto, K. Reddy, E. A. Lumpkin, C. L. Stucky and A. Patapoutian, *Nature*, 2014, **509**, 622.

7. S. Raspopovic, M. Capogrosso, F. M. Petrini, M. Bonizzato, J. Rigosa, G. Di Pino, J. Carpaneto, M. Controzzi, T. Boretius, E. Fernandez, G. Granata, C. M. Oddo, L. Citi, A. L. Ciancio, C. Cipriani, M. C. Carrozza, W. Jensen, E. Guglielmelli, T. Stieglitz, P. M. Rossini and S. Micera, *Sci. Transl. Med.*, 2014, **6**, 222ra19.
8. L. R. Hochberg, D. Bacher, B. Jarosiewicz, N. Y. Masse, J. D. Simeral, J. Vogel, S. Haddadin, J. Liu, S. S. Cash, P. van der Smagt and J. P. Donoghue, *Nature*, 2012, **485**, 372.
9. M. Ortiz-Catalan, B. Hakansson and R. Branemark, *Sci. Transl. Med.*, 2014, **6**, 257re6.
10. B. C. Tee, A. Chortos, A. Berndt, A. K. Nguyen, A. Tom, A. McGuire, Z. C. Lin, K. Tien, W. G. Bae, H. Wang, P. Mei, H. H. Chou, B. Cui, K. Deisseroth, T. N. Ng and Z. Bao, *Science*, 2015, **350**, 313.
11. S. N. Flesher, J. L. Collinger, S. T. Foldes, J. M. Weiss, J. E. Downey, E. C. Tyler-Kabara, S. J. Bensmaia, A. B. Schwartz, M. L. Boninger and R. A. Gaunt, *Sci. Transl. Med.*, 2016, **8**, 361ra141.
12. C. Bartolozzi, L. Natale, F. Nori and G. Metta, *Nat. Mater.*, 2016, **15**, 921.
13. D. W. Tan, M. A. Schiefer, M. W. Keith, J. R. Anderson, J. Tyler and D. J. Tyler, *Sci. Transl. Med.*, 2014, **6**, 257ra138.
14. D. Rus and M. T. Tolley, *Nature*, 2015, **521**, 467.
15. T. Someya, Z. Bao and G. G. Malliaras, *Nature*, 2016, **540**, 379.
16. S. Lee, A. Reuveny, J. Reeder, S. Lee, H. Jin, Q. Liu, T. Yokota, T. Sekitani, T. Isoyama, Y. Abe, Z. Suo and T. Someya, *Nat. Nanotechnol.*, 2016, **11**, 472.
17. C. Wang, D. Hwang, Z. Yu, K. Takei, J. Park, T. Chen, B. Ma and A. Javey, *Nat. Mater.*, 2013, **12**, 899.
18. C. Walsh, *Nat. Rev. Mater.*, 2018, DOI: DOI: 10.1038/s41578-018-0011-1.
19. A. K. Bansal, S. Hou, O. Kulyk, E. M. Bowman and I. D. Samuel, *Adv. Mater.*, 2015, **27**, 7638.
20. Z. Lin, J. Chen, X. Li, Z. Zhou, K. Meng, W. Wei, J. Yang and Z. L. Wang, *ACS Nano*, 2017, **11**, 8830.
21. M. Shi, J. Zhang, H. Chen, M. Han, S. A. Shankaregowda, Z. Su, B. Meng, X. Cheng and H. Zhang, *ACS Nano*, 2016, **10**, 4083.
22. B. Xu, A. Akhtar, Y. Liu, H. Chen, W. H. Yeo, S. I. Park, B. Boyce, H. Kim, J. Yu, H. Y. Lai, S. Jung, Y. Zhou, J. Kim, S. Cho, Y. Huang, T. Bretl and J. A. Rogers, *Adv. Mater.*, 2016, **28**, 4462.
23. S. Imani, A. J. Bandodkar, A. M. Mohan, R. Kumar, S. Yu, J. Wang and P. P. Mercier, *Nat. Commun.*, 2016, **7**, 11650.
24. J. Kim, M. Lee, H. J. Shim, R. Ghaffari, H. R. Cho, D. Son, Y. H. Jung, M. Soh, C. Choi, S. Jung, K. Chu, D. Jeon, S. T. Lee, J. H. Kim, S. H. Choi, T. Hyeon and D. H. Kim, *Nat. Commun.*, 2014, **5**, 5747.
25. J. Chen, G. Zhu, J. Yang, Q. Jing, P. Bai, W. Yang, X. Qi, Y. Su and Z. L. Wang, *ACS Nano*, 2015, **9**, 105.
26. Y. Lee, S. H. Cha, Y. W. Kim, D. Choi and J. Y. Sun, *Nat. Commun.*, 2018, **9**, 1804.
27. X. Wang, Z. Liu and T. Zhang, *Small*, 2017, **13**, 1602790.
28. S. Wang, J. Y. Oh, J. Xu, H. Tran and Z. Bao, *Acc. Chem. Res.*, 2018, DOI: DOI: 10.1021/acs.accounts.8b00015.
29. X. Wang, L. Dong, H. Zhang, R. Yu, C. Pan and Z. L. Wang, *Adv. Sci.*, 2015, **2**, 1500169.
30. J. Wang, M.-F. Lin, S. Park and P. S. Lee, *Mater. Today*, 2018, DOI: DOI: 10.1016/j.mattod.2017.12.006.
31. Y. Liu, K. He, G. Chen, W. R. Leow and X. Chen, *Chem. Rev.*, 2017, **117**, 12893.
32. T. Q. Trung and N. E. Lee, *Adv. Mater.*, 2016, **28**, 4338.
33. H. Jang, Y. J. Park, X. Chen, T. Das, M. S. Kim and J. H. Ahn, *Adv. Mater.*, 2016, **28**, 4184.
34. Y. Zang, F. Zhang, C.-a. Di and D. Zhu, *Mater. Horiz.*, 2015, **2**, 140.
35. X. Liao, X. Yan, P. Lin, S. Lu, Y. Tian and Y. Zhang, *ACS Appl. Mater. Interfaces*, 2015, **7**, 1602.
36. K. K. Kim, S. Hong, H. M. Cho, J. Lee, Y. D. Suh, J. Ham and S. H. Ko, *Nano Lett.*, 2015, **15**, 5240.
37. Y. Wei, S. Chen, X. Yuan, P. Wang and L. Liu, *Adv. Funct. Mater.*, 2016, **26**, 5078.
38. K. Y. Chun, Y. J. Son, E. S. Jeon, S. Lee and C. S. Han, *Adv. Mater.*, 2018, **30**, e1706299.
39. Y. Cai, J. Shen, Z. Dai, X. Zang, Q. Dong, G. Guan, L. J. Li, W. Huang and X. Dong, *Adv. Mater.*, 2017, **29**, 1606411.
40. Y. R. Jeong, H. Park, S. W. Jin, S. Y. Hong, S.-S. Lee and J. S. Ha, *Adv. Funct. Mater.*, 2015, **25**, 4228.
41. N. Luo, Y. Huang, J. Liu, S. C. Chen, C. P. Wong and N. Zhao, *Adv. Mater.*, 2017, **29**, 1702675.
42. X. Wu, Y. Han, X. Zhang, Z. Zhou and C. Lu, *Adv. Funct. Mater.*, 2016, **26**, 6246.
43. H. B. Yao, J. Ge, C. F. Wang, X. Wang, W. Hu, Z. J. Zheng, Y. Ni and S. H. Yu, *Adv. Mater.*, 2013, **25**, 6692.
44. C. Mu, Y. Song, W. Huang, A. Ran, R. Sun, W. Xie and H. Zhang, *Adv. Funct. Mater.*, 2018, **28**, 1707503.
45. L. Pan, A. Chortos, G. Yu, Y. Wang, S. Isaacson, R. Allen, Y. Shi, R. Dauskardt and Z. Bao, *Nat. Commun.*, 2014, **5**, 3002.
46. X. Wang, Y. Gu, Z. Xiong, Z. Cui and T. Zhang, *Adv. Mater.*, 2014, **26**, 1336.
47. B. Zhu, Z. Niu, H. Wang, W. R. Leow, H. Wang, Y. Li, L. Zheng, J. Wei, F. Huo and X. Chen, *Small*, 2014, **10**, 3625.
48. H. H. Chou, A. Nguyen, A. Chortos, J. W. To, C. Lu, J. Mei, T. Kurosawa, W. G. Bae, J. B. Tok and Z. Bao, *Nat. Commun.*, 2015, **6**, 8011.
49. H. Park, Y. R. Jeong, J. Yun, S. Y. Hong, S. Jin, S. J. Lee, G. Zi and J. S. Ha, *ACS Nano*, 2015, **9**.
50. Y. Yang, H. Zhang, Z. H. Lin, Y. S. Zhou, Q. Jing, Y. Su, J. Yang, J. Chen, C. Hu and Z. L. Wang, *ACS Nano*, 2013, **7**, 9213.
51. D. Kang, P. V. Pikhitsa, Y. W. Choi, C. Lee, S. S. Shin, L. Piao, B. Park, K. Y. Suh, T. I. Kim and M. Choi, *Nature*, 2014, **516**, 222.
52. B. Park, J. Kim, D. Kang, C. Jeong, K. S. Kim, J. U. Kim, P. J. Yoo and T. I. Kim, *Adv. Mater.*, 2016, **28**, 8130.
53. B. Park, S. Lee, H. Choi, J. U. Kim, H. Hong, C. Jeong, D. Kang and T. I. Kim, *Nanoscale*, 2018, **10**, 4354.
54. S. Gong, W. Schwalb, Y. Wang, Y. Chen, Y. Tang, J. Si, B. Shirinzadeh and W. Cheng, *Nat. Commun.*, 2014, **5**, 3132.
55. C. Pang, G. Y. Lee, T. I. Kim, S. M. Kim, H. N. Kim, S. H. Ahn and K. Y. Suh, *Nat. Mater.*, 2012, **11**, 795.
56. S. Baik, N. Kim, T.-i. Kim, H. Chae, K. H. Kim, C. Pang and K.-Y. Suh, *Curr. Appl. Phys.*, 2015, **15**, 274.
57. J. Park, Y. Lee, J. Hong, Y. Lee, M. Ha, Y. Jung, H. Lim, S. Y. Kim and H. Ko, *ACS Nano*, 2014, **8**, 12020.
58. J. Park, Y. Lee, S. Lim, Y. Lee, Y. Jung, H. Lim and H. Ko, *BioNanoSci.*, 2014, **4**, 349.
59. C. C. Kim, H. H. Lee, K. H. Oh and J. Y. Sun, *Science*, 2016, **353**, 682.
60. A. Zimmerman, L. Bai and D. D. Ginty, *Science*, 2014, **346**, 950.
61. X. Liao, Q. Liao, X. Yan, Q. Liang, H. Si, M. Li, H. Wu, S. Cao and Y. Zhang, *Adv. Funct. Mater.*, 2015, **25**, 2395.
62. C. W. Lin, Z. Zhao, J. Kim and J. Huang, *Sci. Rep.*, 2014, **4**, 3812.
63. Z. Li, H. Liu, C. Ouyang, W. Hong Wee, X. Cui, T. Jian Lu, B. Pingguan-Murphy, F. Li and F. Xu, *Adv. Funct. Mater.*, 2016, **26**, 165.
64. R. Holm and E. A. Holm, *Electric contacts: theory and application*, Springer-Verlag Berlin Heidelberg, New York, New York, 1967.
65. E. S. Dellon, R. Mourey and A. L. Dellon, *Plast. Reconstr. Surg.*, 1992, **90**, 112.
66. K. S. Novoselov, A. K. Geim, S. V. Morozov, D. Jiang, Y. Zhang, S. V. Dubonos, I. V. Grigorieva and A. A. Firsov, *Science*, 2004, **306**, 666.